

The N^* Physics Program at Jefferson Lab

Volker D. Burkert
(for the CLAS Collaboration)

Jefferson Laboratory
12000 Jefferson Avenue, Newport News, VA23606

*

Abstract Recent measurements of nucleon resonance transition form factors with CLAS at Jefferson Lab are discussed. The new data confirm the assertion of the symmetric constituent quark model of the Roper as the first radial excitation of the nucleon. The data on high Q^2 $n\pi^+$ production better constrain the branching ratios $\beta_{N\pi}$ and $\beta_{N\eta}$ for the $S_{11}(1535)$. For the first time, the longitudinal transition amplitude to the $S_{11}(1535)$ was extracted from the $n\pi^+$ data. Also, new results on the transition amplitudes for the $D_{13}(1520)$ resonance are presented showing a rapid transition from helicity 3/2 dominance seen at the real photon point to helicity 1/2 dominance at higher Q^2 . I also discuss aspects of the search for new excited nucleon states in strangeness photoproduction.

Key words nucleon resonances, transition form factors, $N\Delta$ transition, Roper, magnetic dipole,

PACS PACS (1.55Fv, 13.60Le, 13.40Gp, 14.20Gk)

1 Introduction

Electroexcitation of nucleon resonances has long been recognized as a sensitive tool in the exploration of the complex nucleon structure at varying distances scales. Resonances play an important role in fully understanding the spin structure of the nucleon. More than 80% of the helicity-dependent integrated total photoabsorption cross section difference (GDH integral) is the result of the $N\Delta(1232)$ transition^[1, 2], and at a photon virtuality $Q^2 = 1$ GeV² more than 50% of the first moment $\Gamma_1^P(Q^2) = \int_0^1 g_1(x, Q^2) dx$ of the spin structure function g_1 for the proton is due to contributions of the resonance region at $W < 2$ GeV^[3], and is crucial for describing the entire Q^2 range of $\Gamma_1^P(Q^2)$ and $\Gamma_1^{P-n}(Q^2)$ for the proton and proton-neutron difference respectively^[4, 5, 6]. Nucleon resonances may also be responsible for significant portion of the orbital angular momentum contributions to the nucleon spin due to the strong excitation of resonances with quark orbital angular momentum $\Delta L_z = 1$ and $\Delta L_z = 2$ in the 2nd and 3rd resonance region.

Studies of nucleon resonances are of interest in their own rights. Studying the systematics of the excitation spectrum is key to understanding the symmetry underlying the nucleon matter. Electroexcitation of resonances allows us to probe the internal structure of the excited

state knowing the structure of the ground state. The most comprehensive predictions of the resonance excitation spectrum come from the various implementation of the symmetric constituent quark model based on broken $SU(6)$ symmetry^[7]. Other models predict a different excitation spectrum, e.g. through a diquark-quark picture, or through dynamical baryon-meson interactions. The different resonance models not only predict different excitation spectra but also different Q^2 dependence of transition form factors. Mapping out the transition form factors will tell us a great deal about the underlying quark or hadronic structure.

The CLAS detector is the first full acceptance instrument with sufficient resolution to measure exclusive electroproduction of mesons with the goal of studying the excitation of nucleon resonances in detail. With the GeV electron beam energy available at JLab, the entire resonance mass region and a wide range in the photon virtuality Q^2 can be studied, and many meson final states are measured simultaneously^[8]. In this talk I discuss recent results from the electroproduction of single pions to determine the transition amplitudes to several well-known states. I will also discuss selected aspects of the search for new excited baryon states.

*e-mail: burkert@jlab.org

2 The $N\Delta(1232)$ transition

An interesting aspect of nucleon structure at low energies is a possible quadrupole deformation of the nucleon's lowest excited state, the $\Delta(1232)$. Such a deformation would be evident in non-zero values of the quadrupole transition amplitude E_{1+} from the nucleon to the $\Delta(1232)$ ^[9]. In models with $SU(6)$ spherical symmetry, the $N\Delta$ transition is simply due to a magnetic dipole M_{1+} mediated by a spin flip, and $E_{1+} = S_{1+} = 0$. Dynamically, quadrupole deformations may arise through the interaction of the photon with the pion cloud^[10, 11] or through the one-gluon exchange mechanism^[12]. Simultaneous description of both R_{EM} and R_{SM} is achieved with dynamical models that include pion-nucleon interactions explicitly, supporting the idea that most of the quadrupole strength in the $N\Delta(1232)$ transition is due to meson effects. At the real photon point over 30% of the transition strength is due to pion effects.

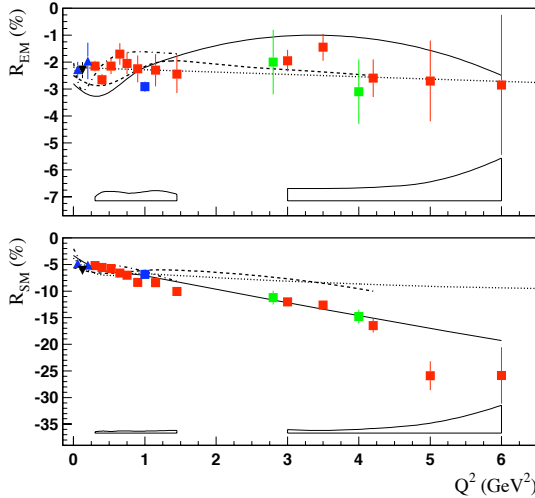


Fig. 1. R_{EM} and R_{SM} extracted from exclusive reactions $p(e, e'p)\pi^0$ using unitary isobar and fixed- t dispersion relations as analysis tools.

At asymptotic momentum transfer, a model-independent prediction of helicity conservation requires $R_{EM} \equiv E_{1+}/M_{1+} \rightarrow +1$. An interpretation of R_{EM} in terms of a quadrupole deformation can thus only be valid at low momentum transfer. Results of the multipole analysis of the JLab data^[18, 19, 20, 21] as well as low Q^2 data from MAMI^[13, 22], Bates^[14] and LEGS^[23] are shown in Fig.1. A consistent picture emerges from these precise data: (1) The magnetic transition form factor drops much faster with Q^2 than the elastic form factor G_m^p which follows approximately the dipole form G_D . (2) R_{EM} remains negative, small and nearly constant in the entire range

$0 < Q^2 < 6 \text{ GeV}^2$. (3) There are no indications that leading pQCD contributions are important as they would result in $R_{EM} \rightarrow +1$ ^[24], and (4) R_{SM} remains negative, and its magnitude rises with Q^2 .

Ultimately, we want to come to a QCD description of these important nucleon structure quantities. In recent years significant effort has been extended towards a Lattice QCD description of the $N\Delta$ transition^[26, 27]. Within the still large error bars, both quenched and unquenched calculations at $Q^2 < 1.5 \text{ GeV}^2$ with pion masses of 400 MeV are consistent with a small negative value of R_{EM} in agreement with the data. For R_{SM} there is a discrepancy at low Q^2 in both quenched and unquenched QCD calculation while the rise in magnitude of R_{SM} with Q^2 observed in the data is quantitatively reproduced in full QCD at $Q^2 > 1 \text{ GeV}^2$.

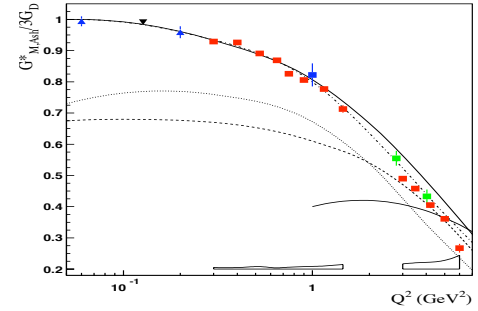


Fig. 2. Magnetic transition form factor G_M^Δ extracted from exclusive reactions pion production, normalized to the dipole form.

3 The Roper resonance $P_{11}(1440)$ - a puzzle resolved

The $N(1440)P_{11}$ resonance (aka "Roper") has been a focus of attention for the last decade, largely due to the inability of the standard constituent quark model to describe basic features such as the mass, photocouplings, and Q^2 evolution. This has led to alternate approaches where the state is treated as a gluonic excitation of the nucleon^[28], or has a small quark core with a large meson cloud^[29], or is a hadronic molecule of a nucleon and a σ meson^[30].

Given these different theoretical concept for the structure of the state, the question "what is the nature of the Roper state?" has been a focus of the N^* program with CLAS. The state couples to both $N\pi$ and $N\pi\pi$ final states. It is also a very wide resonance with about 350 MeV total width. Therefore single and double pion electroproduction data covering a large range in the invariant mass W , with full center-of-mass angular coverage are key

in extracting the transition form factors in a large range of Q^2 . As an isospin $I = \frac{1}{2}$ state, the $P_{11}(1440)$ couples more strongly to $n\pi^+$ than to $p\pi^0$. Also contributions of the high energy tail of the $\Delta(1232)$ are much reduced in that channel due to the $I = \frac{3}{2}$ nature of the $\Delta(1232)$.

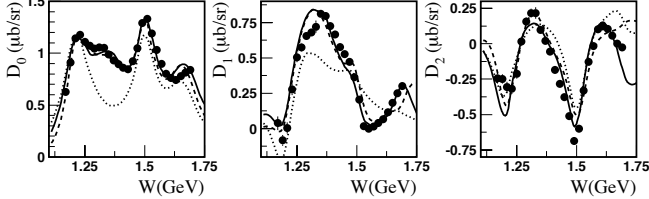


Fig. 3. W dependence of the three lowest Legendre moments from $n\pi^+$ angular distributions at fixed $Q^2 = 2.05 \text{ GeV}^2$. The dotted line indicates the cross section when the amplitudes of the $P_{11}(1440)$ are set equal 0.

A large sample of differential cross sections and polarized beam asymmetry data from CLAS^[33] have been analyzed using the fixed- t dispersion relations approach (DR) and the unitary isobar model (UIM)^[32]. Some of the features of the data may best be seen in the Legendre moments determined in fits to Response functions can be expressed in terms of Legendre polynomials, e.g. the azimuthal angle independent part of the differential cross section can be written as:

$$\sigma_T + \epsilon\sigma_L = \sum_{\ell=0}^{\infty} D_{\ell}^{T+L} P_{\ell}(\cos\Theta_{\pi}^*).$$

Figure 3 shows the lowest Legendre moments for this response functions. The transverse and longitudinal electro-coupling amplitudes $A_{1/2}$ and $S_{1/2}$ of the transition to the $N(1440)P_{11}$ resonance are extracted from fits to the data^[34]. They are shown in Fig. 4.

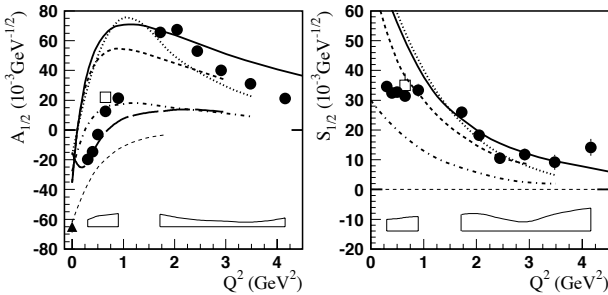


Fig. 4. Transverse electrocoupling amplitude for the Roper $P_{11}(1440)$ (left panel). The full circles are the new CLAS results. The squares are previously published results of fits to CLAS data at low Q^2 . The right panel shows the longitudinal amplitude. The bold curves are all relativistic light front quark model calculations^[38]. The thin solid line is a non-relativistic quark model with a

vector meson cloud^[29], and the thin dashed line is for a gluonic excitation^[28].

At the real photon point $A_{1/2}$ is negative. The CLAS results show a fast rise of the amplitude with Q^2 and a sign change near $Q^2 = 0.5 \text{ GeV}^2$. At $Q^2 = 2 \text{ GeV}^2$ the amplitude has about the same magnitude but opposite sign as at $Q^2 = 0$. It slowly falls off at high Q^2 . This remarkable behavior of a sign change with Q^2 has not been seen before for any nucleon. The longitudinal coupling $S_{1/2}$ is smaller than the transverse one. The first results for the transition form factors of the Roper have recently been obtained in unquenched QCD^[39]. The hybrid baryon model is clearly ruled out for both amplitudes. At high Q^2 both amplitudes are qualitatively described by the light front quark models, which strongly suggests that the Roper is indeed a radial excitation of the nucleon. The low Q^2 behavior is not well described by the LF models and they fall short of describing the amplitude at the photon point. This indicates that important contributions, e.g. meson-baryon interactions at large distances may be missing. In the light front system the Dirac and Pauli form factors F_1 and F_2 can be interpreted as two-dimensional charge densities^[36]. Figure 5 shows the transition charge density in transverse impact parameter space.

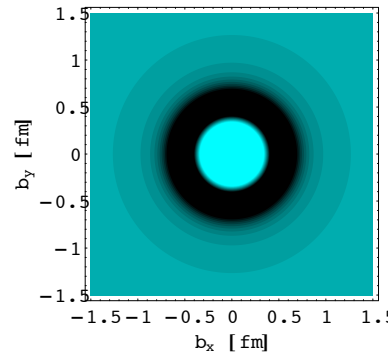


Fig. 5. Transverse transition charge densities in the light front system for the proton to Roper transition in the light-front helicity $+1/2 \rightarrow +1/2$. The light area indicates dominance of up quarks (positive charge), the dark area is due to down quarks (negative charge).

4 The $N(1535)S_{11}$ state

This state has been studied in the $p\eta$ channel where it appears as a rather isolated resonance near the $N\eta$ threshold. Data from CLAS^[40, 41] and Hall C^[42] have

provided a consistent picture of the Q^2 evolution obtained from η electroproduction data alone. There are two remaining significant uncertainties that need to be examined. The first one is due to the branching ratio of the $S_{11}(1535) \rightarrow p\eta$, the second one is due to the lack of precise information on the longitudinal coupling, which in the $p\eta$ channel is usually neglected.

The PDG gives a range of $\beta_{N\eta}^{PDG} = 0.45 - 0.60$. Since this state practically does not couple to channels other than $N\eta$ and $N\pi$, a measurement of the reaction $ep \rightarrow e\pi^+n$ will reduce this uncertainty. Also, the $N\pi$ final state is much more sensitive to the longitudinal amplitude due to a strong $S_{11} - P_{11}$ interference term present in the $N\pi$ channel. Adjusting $\beta_{N\pi} = 0.45$ and $\beta_{N\eta} = 0.45$ brings the two data sets into excellent agreement as shown in Fig. 6.

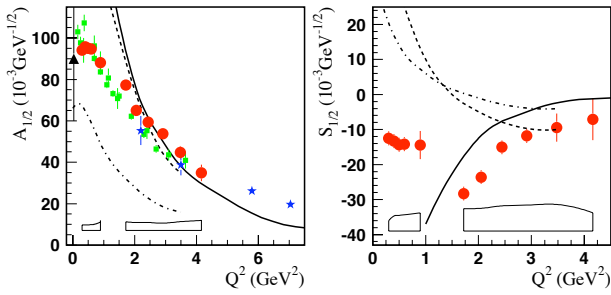


Fig. 6. The transition amplitude $A_{1/2}$ for the $S_{11}(1535)$. The big full circles are from the analysis of the CLAS $n\pi^+$ and $p\pi^0$ data^[34, 35]. The other data are from the analysis of $p\eta$ data^[40, 41, 42, 43]. The theory curves are from various constituent quark models^[46, 47, 48, 49, 58].

An important advantage of the $N\pi$ channel is that it is also sensitive to the longitudinal transition amplitude which is due to a significant $s - p$ wave interference with the nearby p -wave amplitude of the $P_{11}(1440)$. This can be seen in the multipole expansion of the Legendre moment D_0^{LT} :

$$D_0^{LT} = \frac{|\vec{q}|}{K} \text{Re}(E_0 + S_{1-}^* + S_0 + M_{1-}^*).$$

5 Helicity structure of the $D_{13}(1520)$

A longstanding prediction^[44] of the dynamical constituent quark model is the rapid helicity switch from the dominance of the $A_{3/2}$ at the real photon point to the dominance of the $A_{1/2}$ amplitude at $Q^2 > 1 \text{ GeV}^2$. In the simple non-relativistic harmonic oscillator model with spin and orbit flip amplitudes only, the ratio of the

two amplitudes is given by:

$$\frac{A_{1/2}^{D_{13}}}{A_{3/2}^{D_{13}}} = \frac{-1}{\sqrt{3}} \left(\frac{\vec{Q}^2}{\alpha} - 1 \right),$$

where α is a constant adjusted to reproduce the ratio at the photon point where $A_{1/2}$ is very small.

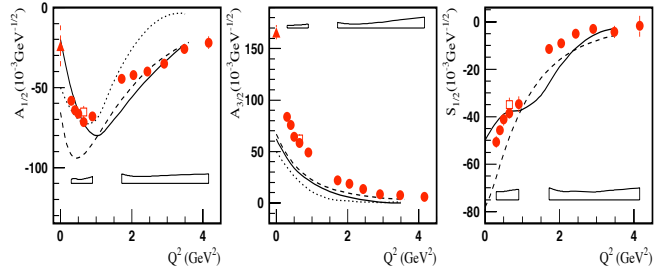


Fig. 7. Electro-coupling amplitudes $A_{1/2}$ (left) and $A_{3/2}$ (middle) and $S_{1/2}$ (right) for the $D_{13}(1520)$. Model curves as in Fig.6.

Figure 7 shows the CLAS results for the electro-couplings. The $A_{3/2}$ amplitude is large at the real photon point and decreasing rapidly in strength with increasing Q^2 . The $A_{1/2}$ amplitude increases rapidly in magnitude with increasing Q^2 , before falling off slowly at $Q^2 > 1 \text{ GeV}^2$. The rapid switch in the helicity structure can best be seen in the helicity asymmetry defined as $A_{hel} = (A_{1/2}^2 - A_{3/2}^2)/(A_{1/2}^2 + A_{3/2}^2)$, and shown in Fig. 8.

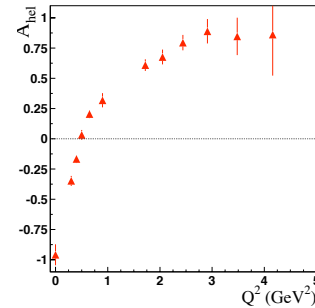


Fig. 8. Helicity asymmetry for the photon induced proton- D_{13} transition vs Q^2 .

6 Search for new nucleon states

The experimental program makes use of the CEBAF Large Acceptance Spectrometer (CLAS)^[50] which provides particle identification and momentum analysis in a polar angle range from 8° to 140° . The photon energy tagger provides energy-marked photons with an energy resolution of $\frac{\sigma(E)}{E} = 10^{-3}$. Other equipment includes a coherent bremsstrahlung facility with a goniometer for diamond crystal positioning and angle control. The facility has been used for linearly polarized photons with

polarizations up to 90%. There are two frozen spin polarized targets, one based on butanol as target material (FROST), and one using HD as a target material (HD-Ice). The latter is currently under construction. FROST has already been operated successfully in longitudinal polarization mode and will be used in transverse polarization mode in 2010. The HD-Ice target will be used as polarized neutron (deuteron) target in scheduled runs in 2010 and 2011. Circularly polarized photons can be generated by scattering the highly polarized electron beam from an amorphous radiator.

It is well understood that measurements of differential cross sections in photoproduction of single pseudoscalar mesons alone results in ambiguous solutions for the contributing resonant partial waves. The N^* program at JLab is therefore aimed at complete, or nearly complete measurements for processes $\vec{\gamma}\vec{p} \rightarrow \pi N$, ηp , $K^+\vec{Y}$ and $\vec{\gamma}\vec{n} \rightarrow \pi N$, $K\vec{Y}$. Complete information can be obtained by using a combination of linearly and circularly polarized photon beams, measurement of hyperon recoil polarization, and the use targets with longitudinal and transverse polarization. The reaction is fully described by 4 complex parity conserving amplitudes, requiring 8 combinations of beam, target, and recoil polarization measurements for an unambiguous extraction of the production amplitudes. If all possible combinations are measured, 16 observables can be extracted. In measurements that involve nucleons in the final state where the recoil polarization is not measured, 7 independent observables can be obtained directly, and the recoil polarization asymmetry P can be inferred from the double polarization asymmetry with linearly polarized beam and transverse target polarization.

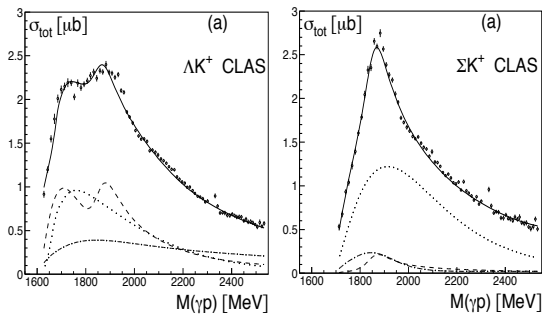


Fig. 9. Integrated total cross section data for $K^+\Lambda$ and $K^+\Sigma^0$ channels. The lines represent the fit results of the Bonn-Gatchina coupled-channel analysis. The dashed line shows the energy-

dependence of the P_{13} partial wave which indicates the presence of two P_{13} resonances at 1720 MeV and at 1900 MeV, respectively. In this analysis, the new $P_{13}(1900)$ contributes a significant fraction to the total $K^+\Lambda$ cross section.

6.1 Search for new states in strangeness channels

A large amount of cross section data have been collected in recent years on the $K\Lambda$ and $K\Sigma$ photoproduction [51, 52]. These data cover the nucleon resonance region in fine steps of about 10 MeV in the hadronic mass W , and nearly the entire polar angle range. The integrated cross section shown in Fig. 9 reveals a strong bump around $W = 1900$ MeV which may be the result of s-channel resonance production. However, more definite conclusions can only be drawn when more polarization observables are included in the analysis. Preliminary results are available from the beam asymmetry in Λ and Σ production with a linearly polarized photon beam. A sample of the data is shown in Fig. 10. Nearly full angle coverage with excellent statistics has been achieved. Beam asymmetry data are particularly important for identifying spin-parity assignment of contributing resonances. These data will span the resonance mass region from threshold up to $W = 2.3$ GeV.

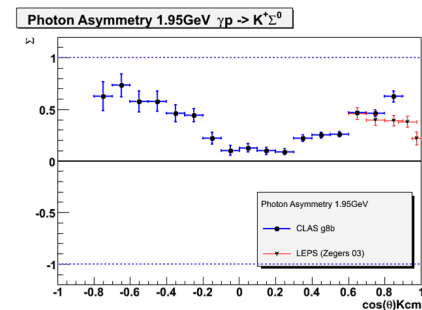


Fig. 10. Sample of preliminary CLAS data for the beam asymmetry of the $K^+\Sigma^0$ final state.

In addition to precise $K\Lambda$ and $K\Sigma$ cross section data recoil polarization and polarization transfer data have been measured [53]. The recoil polarization data in the $K^+\Lambda$ sector showed a highly unexpected behavior: The spin transfer from the circularly polarized photon to the Λ hyperon is complete, leaving the Λ hyperon 100% polarized, as can be seen in Fig. 11. The quadratic sum of all polarization components $R^2 \equiv P^2 + C_x^2 + C_z^2$, which has an upper bound of 1, is consistent with $R^2 = 1$ throughout the region covered by measurement. At first glance this result seems adverse to the idea that the $K\Lambda$ final state has a significant component of N^* resonance associated

with. However, the analysis of the combined CLAS differential cross section and polarization transfer data by the Bonn-Gatchina group ^[55] shows strong sensitivity to a $P_{13}(1900)$ candidate state. The decisive ingredient in this analysis are the CLAS spin transfer coefficients C_x and C_z . Note that the peak observed in the $K^+\Lambda$ data seen near 1900 MeV in Fig. 9 was originally attributed to a $D_{13}(1900)$ resonance before the spin transfer data were included in the fit. A $P_{13}(1900)$ is listed as a 2-star candidate state in the 2008 edition of the RPP ^[56]. If this assignment is confirmed in future analyses which should include additional polarization data, the existence of a $N(1900)P_{13}$ state would be strong evidence against the quark-diquark model ^[57], but would support the symmetric $SU(6)$ constituent quark model. ^[58]

First differential cross sections of the channel $\gamma p \rightarrow K^*\Sigma^+$, covering the mass range $W > 2100$ MeV have been measured recently ^[54]. Several other strangeness channels such as $\gamma n \rightarrow K^0\Lambda$, $K^*\Lambda$, $K^0\Sigma^0$, $K^+\Sigma^-$, and $K^+\Sigma^-(1385)$ are currently being studied to search for new states on neutron targets using circularly and linearly polarized photon beams. For most of these channels a complete kinematical reconstruction in the neutron rest frame is possible, thus eliminating the effect of Fermi motion in the deuteron nucleus. Recoil polarization measurements in all hyperon final states are also available for the analysis.

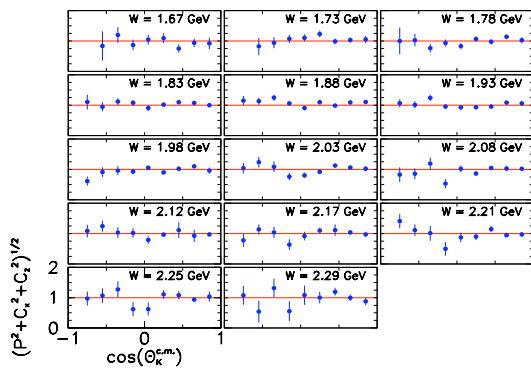


Fig. 11. Spin transfer from the polarized photon to the final state Λ . The spin transfer data were fitted by the Bonn-Gatchina group simultaneously with the CLAS $K^+\Lambda$ and $K^+\Sigma$ differential cross section data. A $P_{13}(1900)$ state is required for the best fit to the cross section and the spin transfer data.

7 Search for new cascade baryons

The production of Ξ hyperons, i.e. strangeness $S = -2$ excited states, presents another promising way of searching for new baryon states. The advantages of cascade hyperon states are due to the expected narrow widths of these states compared to $S = 0$, and $S = -1$ resonances. Possible production mechanisms include t-channel K or K^* exchanges on proton targets with an excited hyperon Y^* (Λ^* or Σ^*) as intermediate state and subsequent decays $Y^* \rightarrow K^+\Xi^*$ and $\Xi^* \rightarrow \Xi\pi$ or $\Xi \rightarrow \Lambda(\Sigma)\bar{K}$. Missing mass technique may be used to search for new states in the reaction $\gamma p \rightarrow K^+K^+X$ if the state is sufficiently narrow to be observed as a peak in the missing mass spectrum. However, an analysis of the final state is needed to assign spin and parity to the state. Data from CLAS taken at 3.6 GeV beam energy show that one can identify the lowest two cascade states this way. ^[60] To identify the higher mass states higher energy is needed.

Another approach to isolate excited cascades and determine their spin-parity, is to measure Ξ with additional particles in the final state. The invariant mass of the $\Xi^0\pi^-$ system is displayed in Fig. 12 and shows the first excited state $\Xi(1530)$ and indications of additional structure near 1620 MeV. A state near that mass is predicted ^[59] as a dynamically generated $\Xi\pi$ system. The data have insufficient statistics and were taken at too low beam energy to allow further investigations. New data taken at 5.7 GeV electron energy and with higher statistics are currently being analyzed, and should allow more definite conclusions on a possible new Ξ state at that mass.

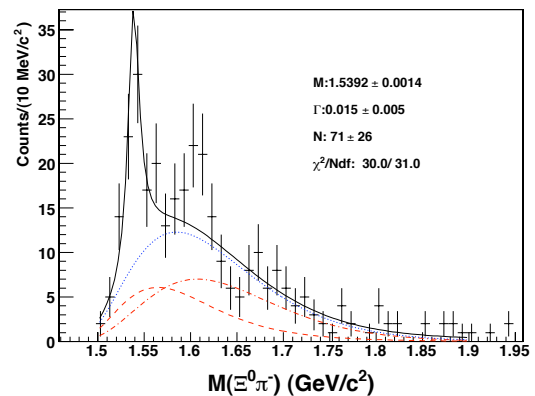


Fig. 12. Invariant mass of the $\Xi\pi^-$ final state. The $\Xi(1530)$ is clearly seen. A possible structure near 1620 MeV could be related to a dynamically generated Ξ state ^[59]

8 Strangeness electroproduction

Significant effort has been devoted to the study of electroproduction of hyperons ^[61, 62] as a complementary means of searching for new excited nucleon states. Figure 13 shows the dependence of the response functions on the hadronic mass W .

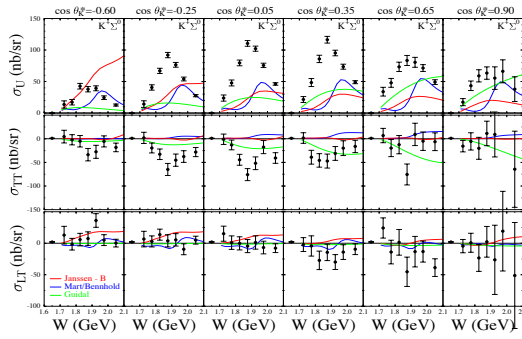


Fig. 13. Separated response functions for $K^+\Sigma^0$ electroproduction. The response function σ_u and σ_{TT} show strong resonance-like structure near $W = 1.9\text{GeV}$, which is not reproduced by any model that include known resonances.

The structure function σ_u shows a resonance-like enhancement near 1.85 - 1.90 GeV in all angle bins. A comparison with model calculations reveals large discrepancies. None of the models that include known nucleon resonance couplings to $K\Sigma$, is able to get the normalization correct. This leaves much room for yet to be identified resonance strength.

9 Outlook

The power of the polarization measurements on the extraction of resonant amplitudes will be brought to bear fully when double and triple polarization data are available making use of longitudinally and transversely polarized proton and neutron targets. Data from CLAS on the polarized proton target (FROST) combined with linearly and circularly polarized photons are currently in the analysis stage. Measurements with transverse polarized proton targets are planned for 2010.

Measurements of polarization observables on polarized neutrons are planned for 2010/2011. Some projected data using the HD-Ice target facility in the CLAS detector are shown in Fig. 14. Single polarization observables

P , Σ and double polarization asymmetries for beam-recoil polarization $O_{y'}$, and target-recoil polarization T_z are shown. Other observables, e.g. target asymmetry T , beam-target asymmetries E , F , and G , H will be measured as well. The projections are for one photon energy bin out of over 25 bins. The solid line is the projection of the kaonMAID code ^[63].

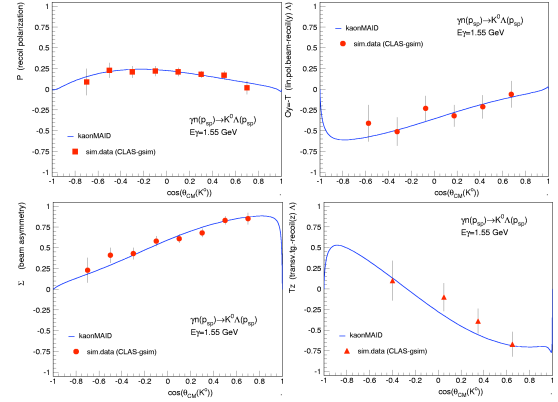


Fig. 14. Simulated data samples for the process $\gamma\bar{n} \rightarrow K_s^0\bar{\Lambda}$. The uncertainties are estimated with the expected run conditions for the upcoming polarized target run using the HD-Ice facility at JLab.

10 Conclusions

With the recent precise data on pion and eta electroproduction, combined with the large coverage in Q^2 , W , and center-of-mass angle, the study of nucleon resonance transitions has become an effective tool in the exploration of nucleon structure in the domain of strong QCD and confinement. We have learned that the $\Delta(1232)$ exhibits an oblate deformation. The multipole ratios R_{EM} and R_{SM} show no sign of approaching the predicted asymptotic behavior, which provides a real challenge for model builders. Lattice QCD simulations do not yet reach the high Q^2 covered by the data. The latest data from CLAS on charged pion production reveal a sign change of the transverse amplitude for the N-Roper transition near $Q^2 = 0.5\text{ GeV}^2$, and give strong evidence for this state as the first radial excitation of the nucleon. The hard transition form factor of the $S_{11}(1535)$ previously observed only in the $p\eta$ channel is confirmed in the $n\pi^+$ channel, which also allows us to extract the so far unmeasured longitudinal amplitude $S_{1/2}$. The $D_{13}(1520)$ clearly exhibits the helicity flip behavior predicted by the constituent quark model. In the light front frame the F_1 and F_2 transition form factors that are obtained from the resonance

helicity amplitudes, can be interpreted as 2-dimensional light cone transition charge densities. This development marks real progress in our understanding of the spatial and spin structure of the nucleon in the domain of strong QCD.

The search for new excited states of the nucleon has entered a new and exciting phase. The main goal of complete or even over determined measurements for pseudo-scalar meson production is now in reach with the availability of energy-tagged linearly and circularly polarized photon beams and the construction of polarized proton

and neutron targets that can be used in longitudinal and in transverse polarization modes. Moreover, for processes involving hyperons in the final state, the hyperon recoil polarization can be measured due to the large analyzing power of the hyperon weak decay $\Lambda \rightarrow p\pi^-$.

Authored by The Southeastern Universities Research Association, Inc. under U.S. DOE Contract No. DE-AC05-84ER40150. The U.S. Government retains a non-exclusive, paid-up, irrevocable, world-wide license to publish or reproduce this manuscript for U.S. Government purposes.

References

- 1 V.D. Burkert, Zh. Li, Phys.Rev.D47, 46, 1993.
- 2 J. Ahrens et al., Phys.Rev.Lett.87, 022003, 2001.
- 3 R. Fatemi et al. (CLAS), Phys. Rev. Lett. 91, 222002, 2003.
- 4 Y. Prok et al. (CLAS), Phys. Lett.B 672, 12, 2009.
- 5 V.D. Burkert and B.L. Ioffe, Phys. Lett. B296, 223, 1992; J. Exp. Theor. Phys. 78, 619, 1994.
- 6 A. Deur et al., Phys. Rev. Lett. 93, 212001, 2004; A. Deur et al., Phys. Rev. D78, 032001, 2008.
- 7 N. Isgur and G. Karl, Phys. Rev. D18, 4187, 1978; Phys. Rev. D19, 2653, 1979.
- 8 V. Burkert and T.-S. H. Lee, Int. J. Phys. E13, 1035, 2004.
- 9 A. Buchmann and E. Henley, Phys. Rev. D65, 073017, 2002.
- 10 T. Sato and T.S. Lee, Phys.Rev.C63, 055201, 2001.
- 11 S.S. Kamalov and S.N. Yang, Phys. Rev. Lett. 83, 4494, 1999.
- 12 R. Koniuk and N. Isgur, Phys. Rev. D21, 1868, 1980.
- 13 S. Stave et al., arXiv:0803.2496 [hep-ex], N.F. Sparveris et al., Phys. Lett. B561, 102, 2007.
- 14 N.F. Sparveris et al., Phys. Rev. Lett. 94, 022003, 2005.
- 15 S.S. Kamalov et al., Phys. Rev. C64, 033201, 2001.
- 16 L. Tiator et al., Eur. Phys. J. A19, 55, 2004.
- 17 D. Drechsel, et al., Eur. Phys. J.A34, 69, 2007.
- 18 V.V. Frolov et al., Phys.Rev.Lett.82:45-48, 1999.
- 19 K. Joo, et al, Phys. Rev. Lett. 88, 122001, 2002.
- 20 M. Ungaro et al., Phys. Rev. Lett.97, 112003, 2006.
- 21 J.J. Kelly et al., Phys. Rev. Lett.95, 102001, 2005.
- 22 R. Beck et al., Phys. Rev. C61, 035204, 2000.
- 23 G. Blampied et al., Phys. Rev. C64, 025203, 2001.
- 24 G. A. Warren, C.E. Carlson, Phys. Rev. D42, 3020, 1990.
- 25 I.G. Aznaurian, Z. Phys. A346, 297, 1993.
- 26 C. Alexandrou et al., Phys. Rev. Lett. 94, 021601, 2005.
- 27 C. Alexandrou et al., Phys. Rev. D77, 085012, 2008.
- 28 Z.P. Li, V. Burkert, Zh. Li; Phys. Rev. D46, 70, 1992.
- 29 F. Cano and P. Gonzales, Phys. Lett. B431, 270, 1998.
- 30 O. Krehl, et al., Phys.Rev.C62,025207, 2000.
- 31 H. Egiyan et al., Phys.Rev.C73,025204, 2006.
- 32 I. Aznauryan, Phys.Rev.C67,015209, 2003.
- 33 K. Park et al., Phys.Rev.C77,015208, 2008.
- 34 I. Aznauryan et al. (CLAS), Phys. Rev. C78, 045209, 2008.
- 35 I. Aznauryan et al., Phys. Rev. C71, 015201; Phys. Rev. C72, 045201, 2005.
- 36 L. Tiator and M. Vanderhaeghen, Phys. Lett. B672, 344-348, 2009.
- 37 N. Mathur et al, Phys.Lett.B605,137, 2005.
- 38 For an overview, see: I. Aznauryan, Phys. Rev. C76, 025212, 2007.
- 39 H.-W. Lin et al, arXiv:0803.3020 [hep-lat]
- 40 R. Thompson et al., Phys. Rev. Lett. 86, 1702, 2001,
- 41 H. Denizli, Phys. Rev. C76, 015204, 2007.
- 42 C.S. Armstrong et al., Phys. Rev. D60, 052004, 1999.
- 43 M.M. Dalton et al., arXiv:0804.3509 [hep-ex]
- 44 F.E. Close and F.J. Gilman, Phys. Lett. B 38, 541, 1972
- 58 S. Capstick and B.D. Keister, Phys. Rev. D51, 3598, 1995.
- 46 E. Pace, G. Salmé, and S. Simula, Few Body Syst. Suppl. 10, 407, 1999.
- 47 D. Merten et al., Eur.Phys.J A14,477, 2002.
- 48 M. Aiello, M.M. Giannini, and E. Santopinto, J. Phys. G24, 753, 1998.
- 49 M. Warns, et al., Z. Phys. C45, 627, 1990.
- 50 B. Mecking et al., Nucl. Instrum. Meth. A503, 513-553, 2003.
- 51 R. Bradford et al., (CLAS), Phys. Rev. C73, 035202, 2006.
- 52 J. W. McNabb et al., (CLAS), Phys. Rev. C69 042201, 2004.
- 53 R. Bradford et al., (CLAS), Phys. Rev. C75, 035205, 2007.
- 54 I. Hleiqawi et al., (CLAS), Phys. Rev. C75, 042201, 2007, Erratum-ibid.C76:039905,2007.
- 55 V.A. Nikonov et al., Phys. Lett. B662, 245, 2008.
- 56 C. Amsler et al., Phys. Lett. B667, 1, 2008.
- 57 E. Santopinto, Phys. Rev. C72, 022201, 2005.
- 58 S. Capstick and W. Roberts, Phys. Rev. D49, 4570, 1994.
- 59 A. Ramos, E. Oset, C. Bennhold, Phys.Rev.Lett.89:252001,2002.
- 60 L. Guo et al., (CLAS), Phys. Rev. C76, 025208, 2007.
- 61 P. Ambrozewicz et al. (CLAS), Phys. Rev. C75, 045203, 2007.
- 62 D. Carman et al., (CLAS), arXiv:0904.3246, 2009.
- 63 F.X. Lee, T. Mart, C. Bennhold, H. Haberzettl, L.E. Wright, Nucl. Phys. A695 (2001) 237